Characterizing proton relaxation times for metallic and magnetic layer-by-layer-coated, DNA-templated nanoparticle chains



2010 Nanotechnology 21 245103

(http://iopscience.iop.org/0957-4484/21/24/245103)

Nanotechnology **21** (2010) 245103 (7pp) doi:10.1088/0957-4484/21/24/245103

# Characterizing proton relaxation times for metallic and magnetic layer-by-layer-coated, DNA-templated nanoparticle chains

**Hamsa Jaganathan**[1], **Richard L Gieseck**[1] **and Albena Ivanisevic**[1,2]

[1] Weldon School of Biomedical Engineering, Purdue University, West Lafayette, IN 47906, USA
[2] Department of Chemistry, Purdue University, West Lafayette, IN 47906, USA

E-mail: albena@purdue.edu

Received 18 February 2010, in final form 29 April 2010
Published 20 May 2010
Online at stacks.iop.org/Nano/21/245103

**Abstract**
Metallic and superparamagnetic DNA-templated nanoparticle (NP) chains are examined as potential imaging agents. Proton relaxation times ($T_1$ and $T_2$) are measured for DNA nanostructures using nuclear magnetic resonance (NMR) spectroscopy. The layer-by-layer (LBL) method was used to encapsulate the DNA-templated NP chains and demonstrated a change in proton relaxation times. Results from this study suggest that LBL-coated, DNA-templated nanostructures can serve as effective imaging agents for magnetic resonance imaging (MRI) applications.

S Online supplementary data available from stacks.iop.org/Nano/21/245103/mmedia

(Some figures in this article are in colour only in the electronic version)

## 1. Introduction

Nanosized structures have been of great interest for use as magnetic resonance imaging (MRI) agents. In recent decades, zero-dimensional iron oxide nanoparticles (NPs) have been demonstrated to be a biocompatible agent that can improve contrast for selective tissues in MRI images [1, 2]. The zero-dimensional nanostructures, however, have low tissue-targeting efficiency and rapid bio-distribution, resulting in an inadequate detection of the MRI signal and image contrast [1]. Currently, this research area is focused on methods to improve the effectiveness of contrast agents by manipulating their structure. For instance, one-dimensional nanostructures have been demonstrated to have higher proton relaxation rates than zero-dimensional nanostructures [2–6]. In addition, Park *et al* determined that one-dimensional, superparamagnetic 'nanoworms' had longer blood circulation times and higher tissue-targeting efficiency when compared to zero-dimensional NPs [6].

In recent years, our group has examined one-dimensional nanostructures templated by DNA [7, 8]. Lambda-phage DNA strands, which serve as biocompatible scaffolds, have lengths in the micron scale and a diameter around 2 nm [9]. Its high aspect ratio (length:diameter), charged nature and recognition properties can be exploited to serve as a soft template for one-dimensional nanostructure formation. DNA has been used as a template for both metallic and magnetic materials, such as silver [10–13], gold [14–16], palladium [17, 18], platinum [19], nickel [20, 21], copper [22], cobalt [23], iron oxide [5, 7] and cobalt iron oxide [24].

Superparamagnetic NPs, such as iron oxide ($Fe_2O_3$) and cobalt iron oxide ($CoFe_2O_4$), are advantageous for MRI applications since they exhibit magnetic moments only in the presence of a large magnetic field. Also, compared to paramagnetic NPs, superparamagnetic NPs have 10- to 1000-fold greater magnetization, aiding in proton relaxation for selective tissues. A short proton relaxation time is needed to produce a strong signal, acquiring contrast enhancement in MRI images [25]. Metallic NPs, such as gold (Au), are advantageous for *in vitro* and *in vivo* applications [26]. Gold is a soft acid that allows for strong binding of numerous chemical functionalities, such as thiols and amines. Since the surface modification of gold is feasible, different ligands and/or

 

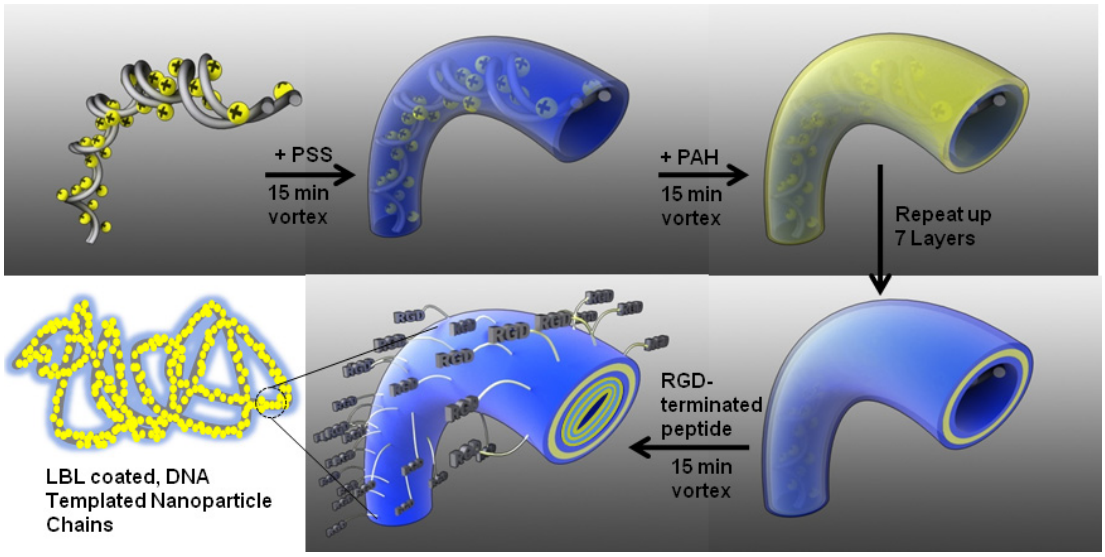


**Scheme 1.** Schematic of layer-by-layer method on DNA-templated nanoparticle chains. Polyelectrolytes (PSS and PAH) are layered up to seven layers with an RGD-terminated poly-L-lysine peptide on the outer surface.

potential drug molecules can be attached for applications in tissue-targeting and drug delivery.

For *in vivo* MRI applications, a biocompatible encapsulation is needed to stabilize the NP-coated DNA structure. DNA can be encapsulated by many different methods, such as using diblock copolymers [27–29], nano- and hydro-gels [30, 31], charged polymers [32], glycopolymers [33], liposomes [34, 35] and the layer-by-layer (LBL) method [36, 37]. The LBL method, or the layering of anionic and cationic polyelectrolytes repeatedly, was chosen to encapsulate DNA nanostructures because it is an inexpensive, feasible procedure to produce a flexible, biocompatible coating. Trubetskoy *et al* was the first to demonstrate that DNA can be coated by the LBL method, exhibiting high structural stability [38]. In addition, many groups have demonstrated that the LBL method provides an effective surface coating for one-dimensional nanostructures [39–45].

Herein, one-dimensional NP chains templated on double-stranded DNA strands are examined as potential imaging agents. First, the longitudinal ($T_1$) and transverse ($T_2$) proton relaxation times for gold, iron oxide and cobalt iron oxide nanostructures are measured through nuclear magnetic resonance (NMR) spectroscopy. Then, a biocompatible encapsulation of the nanostructures is constructed through the LBL method (scheme 1) and the change in proton relaxation times is measured. NMR was used to measure $T_1$ and $T_2$ times for the nanostructures since it exhibits a higher sensitivity than MRI. Therefore, the results collected from NMR measurements provide an initial understanding of the nanostructure's relaxation properties.

## 2. Results and discussion

### *2.1. Relaxation times for DNA-templated nanoparticle chains*

Poly-L-lysine-coated gold NPs (5 nm) were purchased from Ted Pella, Inc. We synthesized both iron oxide and cobalt iron oxide NPs following a protocol from Li *et al* [46] and which results in cationically coated NPs with pyrrolidinone. DNA-templated NP chains were fabricated as previously described in Kinsella *et al* [8]. The structural formation has been studied extensively by circular dichroism spectroscopy and atomic force microscopy [47]. Transmission electron microscope (TEM) images for gold, iron oxide and cobalt iron oxide NPs exhibited agglomeration (figures 1(A)–(C)). DNA-templated NP chains for gold, iron oxide and cobalt iron oxide are flexible when placed in buffer solutions which can tangle if not stretched on surfaces (figures 1(D)–(F)). While iron oxide and cobalt iron oxide NPs demonstrated high NP coating along the DNA strand, gold NPs aligned dispersely along DNA. The observed particle spacing among gold NPs along DNA may be due to the uniformity of the poly-L-lysine monolayer on the NP surfaces [48].

Measuring the relaxation times for the NP chains is important in order to understand their effectiveness as imaging agents for MRI applications. A Bruker DPX300 NMR was used to characterize the longitudinal ($T_1$) and transverse ($T_2$) times for these nanostructures since it is more sensitive than clinical MRI instruments (figure 2). A short relaxation time ($T_1$ or $T_2$) is needed in order to acquire a strong signal, providing contrast in $T_1$- and $T_2$-weighted images.

Since proton relaxation of imaging agents is concentration-dependent, $T_1$ and $T_2$ times for gold, iron oxide and cobalt iron oxide NPs decreased as the NP concentration increased. The observed long relaxation times for gold NPs are equal to the values obtained for the pure solvent, $D_2O$. At a concentration of 1 mg $ml^{-1}$, relaxation times for the superparamagnetic NPs could not be measured. The rate of sedimentation of the NPs was rapid and the $D_2O$ signal could not be locked in the NMR system.

At a low mass ratio of 1:1 DNA:NP, $T_1$ and $T_2$ times were faster than the relaxation times for NPs alone. The proton relaxations observed for DNA-templated gold NP chains may be due to the DNA linking [49] and the inter-particle spacing [50], which has been demonstrated to enhance the

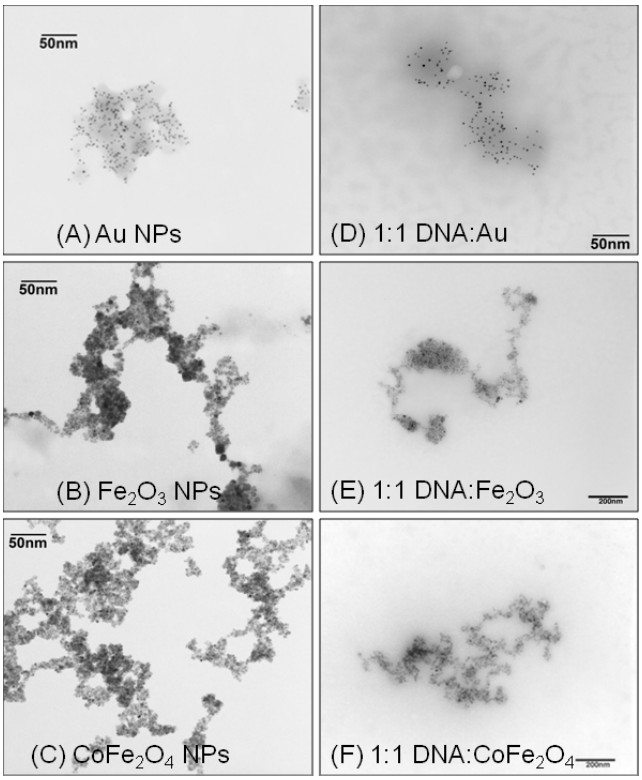


**Figure 1.** TEM images of (A) gold, (B) iron oxide and (C) cobalt iron oxide nanoparticles, along with images of DNA scaffolds of (D) gold, (E) iron oxide and (F) cobalt iron oxide nanoparticles.

collective electromagnetic properties. For superparamagnetic NP chains, the fast relaxation times may be due to the addition of DNA. It has been previously demonstrated that the longitudinal relaxivity of gadolinium increased after the attachment of DNA [51, 52]. Furthermore, Byrne *et al* determined that magnetic relaxivity was enhanced when iron oxide NPs were covalently bound to single-stranded DNA [5]. Results from figure 2 demonstrate that proton relaxation times for iron oxide and cobalt iron oxide nanoparticles are shortened when electrostatically interacting with double-stranded DNA.

The alignment of the superparamagnetic NPs may also affect the change in the relaxation times. For example, Park *et al* observed that their superparamagnetic 'nanoworms' exhibited a higher relaxivity than dispersed NPs alone due to the collective magnetic behavior of aligned NPs [6]. This similar collective magnetic behavior is exhibited by the superparamagnetic NPs arranged along the DNA strands [24], aiding in the fast longitudinal and transverse relaxation times. In figure 2, both $T_1$ and $T_2$ times shortened considerably for mass ratios of 1:5 and 1:10 DNA:NP due to the increase in NP concentration. We have previously demonstrated that, when one uses mass ratios greater than 1:1 DNA:NP, this results in the fabrication of unstable structures. In such cases we have observed NP aggregation and collected spectroscopic evidence that DNA denaturation occurs [47]. At a mass ratio of 1:25 DNA:NP, the sedimentation rate was rapid and relaxation times could not be measured for the superparamagnetic NP chains. Complete NMR data is provided in the supplementary information (available at stacks.iop.org/Nano/21/245103/mmedia).

### *2.2. Relaxation times for LBL-coated, DNA-templated nanoparticle chains*

After observing that the 1:1 DNA:NP mass ratio provided fast relaxation times, DNA-templated NP chains with 1:1 DNA:NP mass ratio were used to construct the LBL surface coating. Poly(styrene sulfonate) (PSS) and poly(allylamine hydrochloride) (PAH) were layered alternately on the DNA-templated NP chains, scheme 1. Fluorescein isothiocyanate (FITC)-labeled PAH was deposited as the eighth polyelectrolyte layer, providing evidence of the LBL coating in the confocal fluorescent images (figures 3(D)–(F)). DNA coated with gold NPs exhibited complete LBL surface coating. Conversely, DNA coated with magnetic NPs exhibited clumping of the polyelectrolytes along the DNA strands. The difference in LBL coating between the magnetic and metallic NP chains is possibly due to the difference in the uniformity of the surface coating of the nanoparticles. A more uniform ligand coating on the gold nanoparticles provided higher LBL

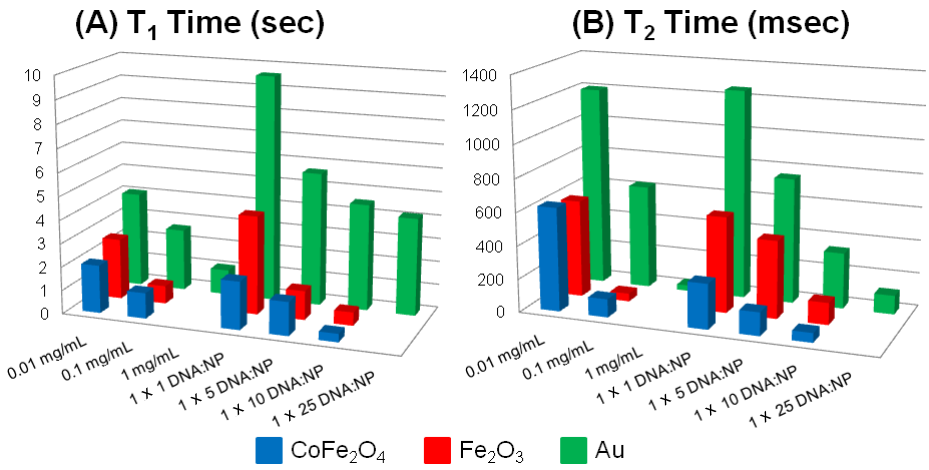


**Figure 2.** (A) Longitudinal ($T_1$) and (B) transverse ($T_2$) relaxation times measured for gold, iron oxide and cobalt iron oxide nanoparticles at different dilutions and different mass ratios with DNA template.

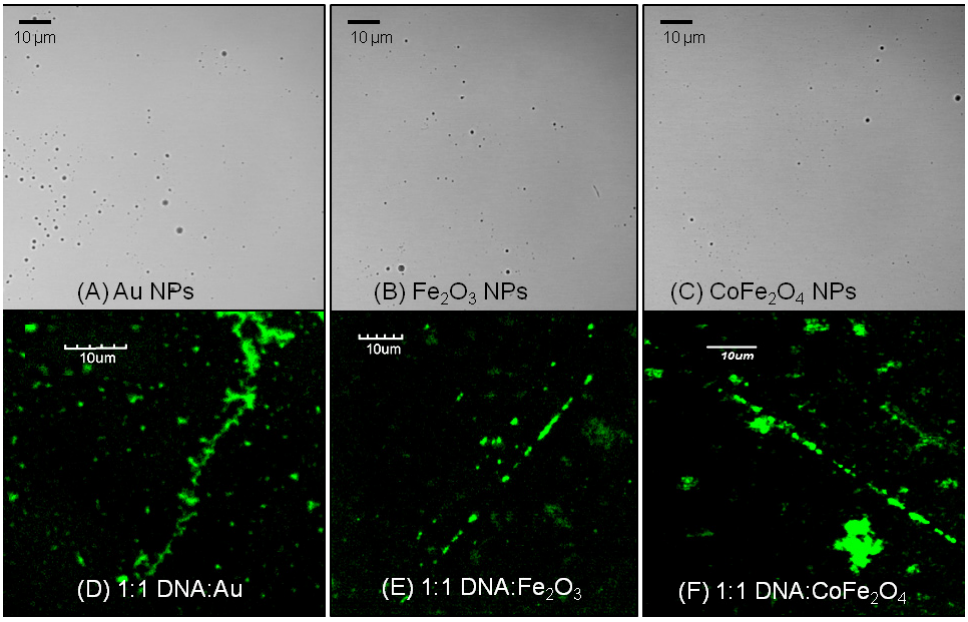


**Figure 3.** The overlayed transmission and confocal fluorescence images exhibited no background fluorescence for (A) gold, (B) iron oxide and (C) cobalt iron oxide NPs. LBL-coated, DNA-templated NP chains for (D) gold, (E) iron oxide and (F) cobalt iron oxide are labeled with FITC on the outermost layer and were stretched on the glass slide.

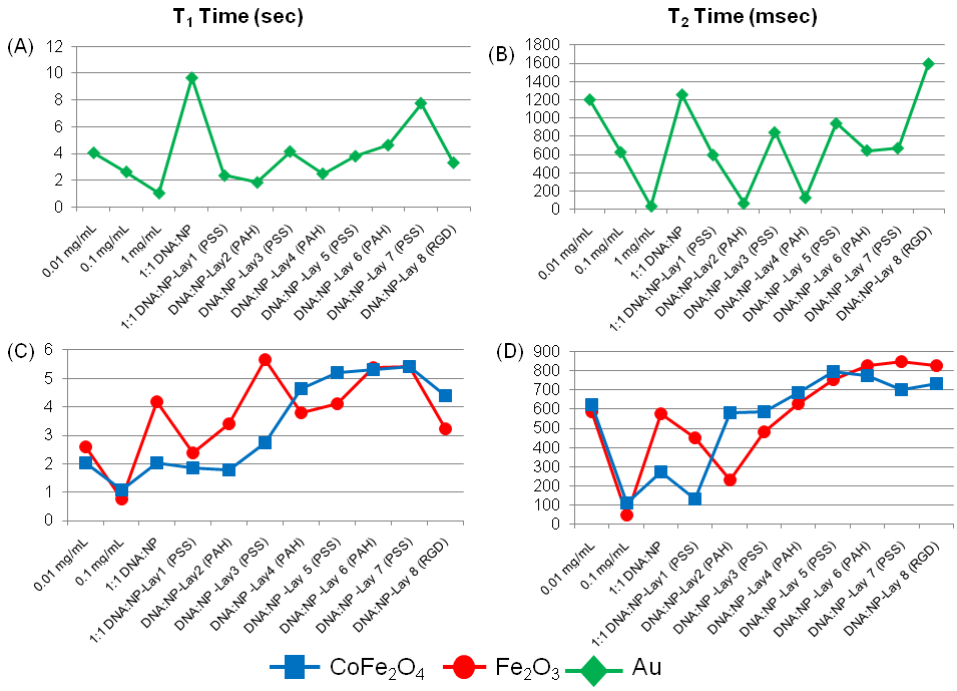


**Figure 4.** Relaxation times after the deposition of each polyelectrolyte layer onto the DNA-templated NP chains. (A) $T_1$ times for gold, (B) $T_2$ times for gold, (C) $T_1$ times for iron oxide and cobalt iron oxide, and (D) $T_2$ times for iron oxide and cobalt iron oxide.

coverage than for the magnetic nanoparticles. Despite the presence of the polyelectrolyte layers on the constructs, the DNA-templated NP chains were able to stretch linearly on the glass substrates, demonstrating the flexible nature of the nanostructures after LBL encapsulation. To illustrate that no background fluorescence was emitted from NPs alone, they were imaged without LBL coating and FITC labeling. The overlayed images from the transmission and fluorescent microscope are displayed in figures 3(A)–(C) for gold, iron oxide and cobalt iron oxide NPs, respectively.

A Bruker DPX300 NMR was used to measure the $T_1$ and $T_2$ relaxation times after each polyelectrolyte layer was deposited onto the DNA-templated NP chains (figure 4). The addition of each polyelectrolyte layer on gold DNA template NP chains shortened $T_1$ times. Conversely, no specific trend was observed for the $T_1$ relaxation times after each layer

was deposited onto the superparamagnetic DNA-templated NP chains. A slightly fluctuating trend is observed for the $T_2$ relaxation times for both types of NP chains. Recently Kim *et al* [53] postulated that the hydrophilic nature of the LBL coating allowed for high accessibility of water molecules to the magnetic agents and increased the efficiency of the proton relaxation. This study was also able to demonstrate that coating NPs using electrostatic interactions provided higher relaxivity than coating NPs using covalent chemistry.

Imaging agents commonly have ligands attached on the outer surface for targeting selective tissues. For example, RGD peptides can be recognized by the integrin receptors on specific tumor cells [54]. As the eighth layer, RGD-terminated poly-L-lysine peptides were added to examine their effect on the relaxation properties. The addition of the RGD peptide demonstrated a 44%, 59% and 67% decrease in the transverse relaxation times for gold, iron oxide and cobalt iron oxide NP chains, respectively. The longitudinal relaxation time, however, exhibited an increase after the addition of the peptide on the DNA-templated NP chains. Since $T_2$ relaxation times were shortened after the addition of the peptide, these DNA-templated NP chains may serve as efficient $T_2$ imaging agents.

## 3. Conclusion

In conclusion, LBL-coated, DNA-templated NP chains for gold, iron oxide and cobalt iron oxide were examined as potential imaging agents. The NP chains were able to retain their stable, flexible structure after coating with polyelectrolytes using a straightforward LBL procedure. Results collected from NMR measurements demonstrated that relaxation times for nanostructures with mass ratios of 1:1 DNA:NP were faster than relaxation times for NPs alone. In addition, NMR studies provided evidence that the LBL coating influenced the proton relaxation times. Findings from this study suggest that LBL-coated, DNA-templated NP chains have the potential to serve as effective imaging agents for MRI applications.

## 4. Methods

### *4.1. Formation of the LBL-coated, DNA-templated nanoparticle chains*

Poly-L-lysine-coated gold NPs (5 nm) were purchased from Ted Pella, Inc. Both iron oxide and cobalt iron oxide NPs (5 nm) were synthesized in the lab, following the protocol from Li *et al* [46], and were cationically coated with pyrrolidinone. In 1X MULTI-CORE™ buffer (Promega), 25 $\mu$l of lambda-phage DNA (Promega: 536 $\mu$g ml$^{-1}$) was added with 25 $\mu$l of NPs (1 mg ml$^{-1}$). After vortexing the solution for 1 h, DNA-templated NP chains were formed. The layer-by-layer method consists of layering the nanostructure using oppositely charged polyelectrolytes. Poly(styrene sulfonate), the anionic polyelectrolyte (Sigma-Aldrich: PSS–MW approx. 70 000), and poly(allylamine hydrochloride), the cationic polymer (Sigma-Aldrich: PAH–MW approx. 70 000), are layered onto the nanostructure. After adding 4 $\mu$l of PSS (1 mg ml$^{-1}$), the solution is vortexed for 15 min at room temperature. Then, 4 $\mu$l of PAH (1 mg ml$^{-1}$) is added as the second layer into the solution, which is also vortexed for 15 min. The addition of PSS and PAH every 15 min continues until seven layers have been established on the nanostructure. This washless process for layer-by-layer encapsulation is discussed further in Bantchev *et al* [55]. After the seventh layer is terminated with the anionic polyelectrolyte, PSS, then the RGD-terminated poly-L-lysine peptide chain is added. The peptide sequence (KKKKKKRGD) was purchased from Biosynthesis Inc. As the eighth layer, 2 $\mu$l of the dissolved peptide (1 $\mu$g ml$^{-1}$) was added.

### *4.2. Nuclear magnetic resonance measurements*

After all the samples were made, 100 $\mu$l of deuterium oxide (Sigma-Aldrich: 99.9 at.%) was added to achieve a total volume of 500 $\mu$l of the sample (leading to a 20% $D_2O$/80% $H_2O$ content). The samples were then degassed by purging with nitrogen gas for 1 min to ensure the elimination of paramagnetic oxygen. Data collected before performing the degassing procedure is shown in the supplementary information (available at stacks.iop.org/Nano/21/245103/mmedia). A Bruker Avance DPX300 (300 MHz), equipped with a 5 mm QNP H1 probe, was used to measure the longitudinal, $T_1$, and the transverse, $T_2$, relaxation times for each sample with a locked signal on $D_2O$. The inversion-recovery pulse sequence was used to measure the longitudinal relaxation times and the Carr–Purcell–Meiboom–Gill (CPMG) pulse sequence was used to measure the transverse relaxation times. A total of eight scans per spectrum were measured for each sample, and the relaxation times and their standard error for the $T_1$ and $T_2$ spectra were collected. Repetition times were always longer than five times the $T_1$ time. A total of eight delays were used to acquire the $T_1$ and $T_2$ spectra. Additionally, in order to ensure that the NMR signal was not saturating the amplifier, the receiver gain for the 2D NMR relaxation time experiments was always set lower than the receiver gain measured for the 1D proton spectrum for each sample. All measurements were recorded at room temperature with no sample spinning.

### *4.3. Transmission electron microscope and confocal fluorescence imaging*

For TEM images, carbon film grids (400 mesh) were used to image NPs and DNA-templated NP chains. Samples were imaged using a Philips CM-100 TEM operated at 100 kV. Images were captured on Kodak SO-163 electron image film. For confocal fluorescence imaging, cleaned glass slides were used to stretch the LBL-coated DNA nanostructures. The eighth layer of the nanostructures contained FITC-labeled PAH for imaging. The stretching procedure for LBL-coated DNA-templated NP chains was adopted from Nakao *et al* [56]. Twenty microliters of NP chain solution was added to the cleaned glass slide surface. Then, 40 $\mu$l of the drop was sucked up slowly by a pipette and this allowed the LBL-coated, DNA-templated NP chains to stretch by air–water interface motion. The sample was set to dry overnight and was then

rinsed with water. Images were collected by using an Olympus (Melville, NY) IX-70 inverted confocal microscope system. The Olympus 60×/1.2 NA water objective with the 488 nm excitation laser was used to image the nanostructures. Images were processed by using Fluoview™ (Olympus, Melville, NY).

## Acknowledgments

This work was supported by NSF under CMMI-0727927. We thank Dr John Harwood from Purdue Interdepartmental NMR Facility for his assistance and training on the Bruker DPX300, Debra Sherman from Purdue University Life Science Microscopy Facility for assistance with TEM, and Professor Thomas Talavage, co-director of Purdue University MRI Facility at InnerVision West, for insightful discussions.

## References

[1] Chouly C, Pouliquen D, Lucet I, Jeune J J and Jallet P 1996 Development of superparamagnetic nanoparticles for MRI: effect of particle size, charge and surface nature on biodistribution *J. Microencapsul.* **13** 245–55

[2] Bai X, Son S J, Zhang S, Liu W, Jordan E K, Frank J A, Venkatesan T and Bok Lee S 2008 Synthesis of superparamagnetic nanotubes as MRI contrast agents and for cell labeling *Nanomedicine* **3** 163–74

[3] Corr S A, Byrne S J, Tekoriute R, Meledandri C J, Brougham D F, Lynch M, Kerskens C, O'Dwyer L and Gun'ko Y K 2008 Linear assemblies of magnetic nanoparticles as MRI contrast agents *J. Am. Chem. Soc.* **130** 4214–5

[4] Nath S, Kaittanis C, Ramachandran V, Dalal N S and Perez J M 2009 Synthesis, magnetic characterization, and sensing applications of novel dextran-coated iron oxide nanorods *Chem. Mater.* **21** 1761–7

[5] Byrne S J, Corr S A, Gun'ko Y K, Kelly J M, Brougham D F and Ghosh S 2004 Magnetic nanoparticle assemblies on denatured DNA show unusual magnetic relaxivity and potential applications for MRI *Chem. Commun.* **22** 2560–1

[6] Park J-H, Maltzahn G V, Zhang L, Schwartz M P, Ruoslahti E, Bhatia S N and Sailor M J 2008 Magnetic iron oxide nanoworms for tumor targeting and imaging *Adv. Mater.* **20** 1630–5

[7] Nyamjav D and Ivanisevic A 2005 Templates for DNA-templated Fe3O4 nanoparticles *Biomaterials* **26** 2749–57

[8] Kinsella J M and Ivanisevic A 2007 DNA-templated magnetic nanowires with different compositions: fabrication and analysis *Langmuir* **23** 3886–90

[9] Whitesides G M, Mathias J P and Seto C T 1991 Molecular self-assembly and nanochemistry: a chemical strategy for the synthesis of nanostructures *Science* **254** 1312–9

[10] Petty J T, Zheng J, Hud N V and Dickson R M 2004 DNA-templated Ag nanocluster formation *J. Am. Chem. Soc.* **126** 5207–12

[11] Sengupta B, Ritchie C M, Buckman J G, Johnsen K R, Goodwin P M and Petty J T 2008 Base-directed formation of fluorescent silver clusters *J. Phys. Chem.* C **112** 18776–82

[12] Shemer G, Krichevski O, Markovich G, Molotsky T, Lubitz I and Kotlyar A B 2006 Chirality of silver nanoparticles synthesized on DNA *J. Am. Chem. Soc.* **128** 11006–7

[13] Wei G, Wang L, Zhou H, Liu Z, Song Y and Li Z 2005 Electrostatic assembly of CTAB-capped silver nanoparticles along predefined [lambda]-DNA template *Appl. Surf. Sci.* **252** 1189–96

[14] Han G, Chari N S, Verma A, Hong R, Martin C T and Rotello V M 2005 Controlled recovery of the transcription of nanoparticle-bound DNA by intracellular concentrations of glutathione *Bioconjug. Chem.* **16** 1356–9

[15] Kundu S, Maheshwari V and Saraf R F 2007 Photolytic metallization of Au nanoclusters and electrically conducting micrometer long nanostructures on a DNA scaffold *Langmuir* **24** 551–5

[16] Fischler M, Sologubenko A, Mayer J, Clever G, Burley G, Gierlich J, Carell T and Simon U 2008 Chain-like assembly of gold nanoparticles on artificial DNA templates via 'click chemistry' *Chem. Commun.* **2** 169–71

[17] Fang C, Fan Y, Kong J M, Zhang G J, Linn L and Rafeah S 2007 DNA-templated preparation of palladium nanoparticles and their application *Sensors Actuators* B **126** 684–90

[18] Richter J, Seidel R, Kirsch R, Mertig M, Pompe W, Plaschke J and Schackert H K 2000 Nanoscale palladium metallization of DNA *Adv. Mater.* **12** 507–10

[19] Seidel R, Colombi Ciacchi L, Weigel M, Pompe W and Mertig M 2004 Synthesis of platinum cluster chains on DNA templates: conditions for a template-controlled cluster growth *J. Phys. Chem.* B **108** 10801–11

[20] Liu Z, Zu Y, Fu Y, Zhang Y and Liang H 2008 Growth of the oxidized nickel nanoparticles on a DNA template in aqueous solution *Mater. Lett.* **62** 2315–7

[21] Bagkar N, Choudhury S, Bhattacharya S and Yakhmi J V 2008 DNA-templated assemblies of nickel hexacyanoferrate crystals *J. Phys. Chem.* B **112** 6467–72

[22] Monson C F and Woolley A T 2003 DNA-templated construction of copper nanowires *Nano Lett.* **3** 359–63

[23] Gu Q and Haynie D T 2008 Palladium nanoparticle-controlled growth of magnetic cobalt nanowires on DNA templates *Mater. Lett.* **62** 3047–50

[24] Kinsella J M and Ivanisevic A 2008 Magnetotransport of one-dimensional chains of CoFe2O4 nanoparticles ordered along DNA *J. Phys. Chem.* C **112** 3191–3

[25] Duguet E, Vasseur S B, Mornet S P and Devoisselle J-M 2006 Magnetic nanoparticles and their applications in medicine *Nanomedicine* **1** 157–68

[26] Agarwal A, Lvov Y, Sawant R and Torchilin V 2008 Stable nanocolloids of poorly soluble drugs with high drug content prepared using the combination of sonication and layer-by-layer technology *J. Control. Release* **128** 255–60

[27] Csaba N, Caamano P, Sanchez A, Dominguez F and Alonso M J 2004 PLGA:poloxamer and PLGA:poloxamine blend nanoparticles: new carriers for gene delivery *Biomacromolecules* **6** 271–8

[28] Ditto A J, Shah P N, Gump L R and Yun Y H 2009 Nanospheres formulated from l-tyrosine polyphosphate exhibiting sustained release of polyplexes and *in vitro* controlled transfection properties *Mol. Pharmaceut.* **6** 986–95

[29] Korobko A V, Backendorf C and van der Maarel J R C 2006 Plasmid DNA encapsulation within cationic diblock copolymer vesicles for gene delivery *J. Phys. Chem.* B **110** 14550–6

[30] Papancea A, Valente A J M, Patachia S, Miguel M G and Lindman B 2007 PVA–DNA cryogel membranes: characterization, swelling, and transport studies *Langmuir* **24** 273–9

[31] Van Thienen T G, Raemdonck K, Demeester J and De Smedt S C 2007 Protein release from biodegradable dextran nanogels *Langmuir* **23** 9794–801

[32] Gu Z, Yuan Y, He J, Zhang M and Ni P 2009 Facile approach for DNA encapsulation in functional polyion complex for triggered intracellular gene delivery: design, synthesis, and mechanism *Langmuir* **25** 5199–208

[33] Srinivasachari S, Liu Y, Zhang G, Prevette L and Reineke T M 2006 Trehalose click polymers inhibit nanoparticle aggregation and promote pDNA delivery in serum *J. Am. Chem. Soc.* **128** 8176–84
[34] Davis S C and Szoka F C 1998 Cholesterol phosphate derivatives: synthesis and incorporation into a phosphatase and calcium-sensitive triggered release liposome *Bioconjug. Chem.* **9** 783–92
[35] Boyer C and Zasadzinski J A 2007 Multiple lipid compartments slow vesicle contents release in lipases and serum *ACS Nano* **1** 176–82
[36] Shchukin D G, Patel A A, Sukhorukov G B and Lvov Y M 2004 Nanoassembly of biodegradable microcapsules for DNA encasing *J. Am. Chem. Soc.* **126** 3374–5
[37] Cavalieri F, Postma A, Lee L and Caruso F 2009 Assembly and functionalization of DNA–polymer microcapsules *ACS Nano* **3** 234–40
[38] Trubetskoy V, Wong S, Subbotin V, Budker V, Loomis A, Hagstrom J and Wolff J 2003 Recharging cationic DNA complexes with highly charged polyanions for *in vitro* and *in vivo* gene delivery *Gene Ther.* **10** 261–71
[39] Liang Z, Susha A S, Yu A and Caruso F 2003 Nanotubes prepared by layer-by-layer coating of porous membrane templates *Adv. Mater.* **15** 1849–53
[40] Kim J, Lee S W, Hammond P T and Shao-Horn Y 2009 Electrostatic layer-by-layer assembled Au nanoparticle/MWNT thin films: microstructure, optical property, and electrocatalytic activity for methanol oxidation *Chem. Mater.* **21** 2993–3001
[41] Magnin D, Callegari V, Matefi-Tempfli S, Matefi-Tempfli M, Glinel K, Jonas A M and Demoustier-Champagne S 2008 Functionalization of magnetic nanowires by charged biopolymers *Biomacromolecules* **9** 2517–22
[42] Lu G, Ai S and Li J 2005 Layer-by-layer assembly of human serum albumin and phospholipid nanotubes based on a template *Langmuir* **21** 1679–82
[43] Hou S, Harrell C C, Trofin L, Kohli P and Martin C R 2004 Layer-by-layer nanotube template synthesis *J. Am. Chem. Soc.* **126** 5674–5
[44] Gu B X, Xu C X, Zhu G P, Liu S Q, Chen L Y, Wang M L and Zhu J J 2009 Layer by layer immobilized horseradish peroxidase on zinc oxide nanorods for biosensing *J. Phys. Chem.* B **113** 6553–7
[45] Lee D, Cohen R E and Rubner M F 2006 Heterostructured magnetic nanotubes *Langmuir* **23** 123–9
[46] Li Z, Chen H, Bao H and Gao M 2004 One-pot reaction to synthesize water-soluble magnetite nanocrystals *Chem. Mater.* **16** 1391–3
[47] Jaganathan H, Kinsella J M and Ivanisevic A 2008 Circular dichroism study of the mechanism of formation of DNA templated nanowires *ChemPhysChem* **9** 2203–6
[48] Wang G and Murray R W 2003 Controlled assembly of monolayer-protected gold clusters by dissolved DNA *Nano Lett.* **4** 95–101
[49] Lazarides A A and Schatz G C 1999 DNA-linked metal nanosphere materials: structural basis for the optical properties *J. Phys. Chem.* B **104** 460–7
[50] Ramakrishna G, Dai Q, Zou J, Huo Q and Goodson T 2007 Interparticle electromagnetic coupling in assembled gold-necklace nanoparticles *J. Am. Chem. Soc.* **129** 1848–9
[51] Cai J, Shapiro E M and Hamilton A D 2009 Self-assembling DNA quadruplex conjugated to MRI contrast agents *Bioconjug. Chem.* **20** 205–8
[52] Caravan P, Greenwood J M, Welch J T and Franklin S J 2003 Gadolinium-binding helix-turn-helix peptides: DNA-dependent MRI contrast agents *Chem. Commun.* **20** 2574–5
[53] Kim J S, Rieter W J, Taylor K M L, An H, Lin W and Lin W 2007 Self-assembled hybrid nanoparticles for cancer-specific multimodal imaging *J. Am. Chem. Soc.* **129** 8962–3
[54] Toublan F J-J, Boppart S and Suslick K S 2006 Tumor targeting by surface-modified protein microspheres *J. Am. Chem. Soc.* **128** 3472–3
[55] Bantchev G, Lu Z and Lvov Y 2009 Layer-by-layer nanoshell assembly on colloids through simplified washless process *J. Nanosci. Nanotechnol.* **9** 396–403
[56] Nakao H, Shiigi H, Yamamoto Y, Tokonami S, Nagaoka T, Sugiyama S and Ohtani T 2003 Highly ordered assemblies of Au nanoparticles organized on DNA *Nano Lett.* **3** 1391–4